Icarus 205 (2010) 296–310

Contents lists available at ScienceDirect

Icarus

journal homepage: www.elsevier.com/locate/icarus

HiRISE observations of gas sublimation-driven activity in Mars' southern polar regions: II. Surficial deposits and their origins

N. Thomas [a,*], C.J. Hansen [b], G. Portyankina [a], P.S. Russell [a]

[a] Physikalisches Institut, Sidlerstr. 5, University of Bern, CH-3012 Bern, Switzerland
[b] Jet Propulsion Laboratory, 4800 Oak Grove Drive, Pasadena, CA 91109, USA

ARTICLE INFO

Article history:
Received 4 November 2008
Revised 1 May 2009
Accepted 28 May 2009
Available online 13 June 2009

Keywords:
Mars
Mars, Polar Geology
Mars, Surface

ABSTRACT

The High Resolution Imaging Science Experiment (HiRISE) onboard Mars Reconnaissance Orbiter (MRO) has been used to monitor the seasonal evolution of several regions at high southern latitudes and, in particular, the jet-like activity which may result from the process described by Kieffer (JGR, 112, E08005, doi:10.1029/2006JE002816, 2007) involving translucent CO_2 ice. In this work, we mostly concentrate on observations of the Inca City (81°S, 296°E) and Manhattan (86°S, 99°E) regions in the southern spring of 2007. Two companion papers, [Hansen et al. this issue] and [Portyankina et al. this issue], discuss the surface features in these regions and specific models of the behaviour of CO_2 slab ice, respectively. The observations indicate rapid on-set of activity in late winter initiating before HiRISE can obtain adequately illuminated images (Ls < 174° at Inca City). Most sources become active within the subsequent 8 weeks. Activity is indicated by the production of dark deposits surrounded by brighter bluer deposits which probably arise from the freezing out of vented CO_2 [Titus et al., 2007. AGU (abstract P41A-0188)]. These deposits originate from araneiform structures (spiders), boulders on ridges, cracks on slopes, and along linear cracks in the slab ice on flatter surfaces. The type of activity observed can often be explained qualitatively by considering the local topography. Some dark fans are observed to shorten enormously in length on a timescale of 18 days. We consider this to be strong evidence that outgassing was in progress at the time of HiRISE image acquisition and estimate a total particulate emission rate of >30 g s^{-1} from a single typical jet feature. Brighter deposits at Inca City become increasingly hard to detect after Ls = 210°. In the Inca City region, the orientations of surficial deposits are topographically controlled. The deposition of dark material also appears to be influenced by local topography suggesting that the ejection from the vents is at low velocity (<10 m s^{-1}) and that a ground-hugging flow process (a sort of "cryo-fumarole") may be occurring. The failure up to this point to obtain a clear detection of outgassing though stereo imaging is consistent with low level transport. The downslope orientation of the deposits may result from the geometry of the vent or from catabatic winds. At many sites, more than one ejection event appears to have occurred suggesting re-charging of the sources. Around Ls = 230°, the brightness of the surface begins to drop rapidly on north-facing slopes and the contrast between the dark deposits and the surrounding surface reduces. This indicates that the CO_2 ice slab is being lost completely in some areas at around this time. By Ls = 280°, at Inca City, the ice slab has effectively gone. CRISM band ratios and THEMIS brightness temperature measurements are consistent with this interpretation.

1. Introduction

1.1. General

The influence of CO_2 sublimation and condensation on the atmosphere and polar caps of Mars was first described and modelled by Leighton and Murray (1966). Sublimation and condensation at the surface was assumed to be the universal mechanism for CO_2 exchange between the atmosphere and the polar caps. However, as described in Hansen et al. (this issue), the Mars Orbiting Camera (MOC; Malin et al., 1998) showed the presence of fan-like dark patches on the surface of the subliming southern polar caps. Kieffer (2000) suggested that the unique properties of CO_2 ice are responsible for this phenomenon which probably results from a type of solid-state greenhouse effect (Matson and Brown, 1989; Piqueux et al., 2003; Kaufmann et al., 2006; Kaufmann, 2007; Kieffer, 2007; Piqueux and Christensen, 2008) involving CO_2 slab ice. By being translucent at optical wavelengths, but relatively opaque at infra-red wavelengths, a thin

* Corresponding author. Fax: +41 31 631 4405.
E-mail addresses: nicolas.thomas@space.unibe.ch (N. Thomas), candice.j.hansen@jpl.nasa.gov (C.J. Hansen), portyankina@space.unibe.ch (G. Portyankina), patrick.russell@space.unibe.ch (P.S. Russell).

0019-1035/$ - see front matter © 2009 Elsevier Inc. All rights reserved.
doi:10.1016/j.icarus.2009.05.030

CO_2 ice sheet (the result of condensation in winter onto a dusty or rocky substrate) can result in solar energy being deposited at the boundary between the ice sheet and the substrate without a ready means of escape. This leads to sublimation at the ice-substrate interface with subsequent pressure build-up. When the pressure becomes sufficient to exploit a weakness in the ice sheet, it is released by venting, effectively producing a jet-like activity. Gas pressure gradients produce a flow from the sub-surface regions surrounding the vent to the vent itself to maintain activity for an, as yet, undetermined time. Dust entrained in the gas flow is also ejected from the vent and is deposited on the surrounding surface. The gas and dust flow under the surface results in erosion which can lead to the development of narrow channels in the substrate. The deposition pattern by the entrained dust should be influenced by the vent geometry, the ejection conditions, the local topography, and local winds. Kieffer (2007) provided a detailed model of the complete process including estimates for the height of the inferred gas jets. Piqueux et al. (2003) linked venting to surface structures by suggesting that "araneiform" (spider-like) structures in the southern polar region had been produced by this process.

This is the second of three papers which describe the surface morphology and sublimation-driven activity in specific areas of the martian south polar region as observed by the High Resolution Imaging Science Experiment (HiRISE) onboard NASA's Mars Reconnaissance Orbiter (MRO) spacecraft. In Hansen et al. (this issue), the appearance of the surface in the "Inca City" and "Manhattan" regions of Mars is described. This includes presentation of the various araneiform ("spider-like") structures observed as well as evidence for control of their appearance by the topography of the underlying substrate. Here, we address the high resolution observations of surface deposits resulting from inferred, sublimation-driven, "jet-like", activity (e.g. Kieffer, 2000; Kieffer et al., 2006; Kieffer, 2007). The deposition patterns of dust entrained in the outflow place constraints on the properties of the outflow. Furthermore, the time evolution of the appearance of these deposits and the relationship of the deposits to the local topography also provides information on the processes involved in forming them. Here, we describe the observations made by HiRISE and discuss their implications with respect to the current paradigms. In Portyankina et al. (this issue), models relating to the sublimation-driven activity process and specifically the timescales for initiation of that activity are presented.

The structure of this contribution is as follows. We refer to Hansen et al. (this issue) for a detailed introduction but note some additional points in the rest of this section. Section 2 discusses the timing of the on-set of activity at the beginning of southern spring and the observed jet sources. In Section 3, we show evidence from HiRISE for the freezing-out of the jet-driving volatiles. We show that not only dust is deposited on the surface during an outburst but we infer that the driving volatile can also freeze and condense onto the surface leaving a visible signature in HiRISE data. This allows us to extend the observations made by CRISM of this phenomenon (Titus et al., 2007) to smaller scales. We then discuss the attempts to observe jets in the act of emitting material and suggest that HiRISE has indeed seen activity in progress although it remains possible to construct an alternative, albeit unlikely, scenario. In Section 5, we present some of the different types of outgassing sources and show that activity need not be obviously related to a surface structure. It will also be apparent from these observations that the centres of the araneiform structures are not necessarily the immediate sources of venting. Section 6 discusses models of the deposition patterns and shows that, for reasonable values, the heights of the jets must be small. Finally, we show how the ejecta deposits return back to the substrate surface after CO_2 sublimation has completed, thereby allowing repetition of the cycle with relatively loose material as a source for further dust entrainment in the following year.

It has been noted (Kieffer, 2007) that there is great diversity and regional variability of observed phenomena within the southern polar region. It should be noted that, as in Hansen et al. (this issue), we consider here only two regions – "Manhattan" and "Inca City" – and we refer to Hansen et al. for a full description including topographic maps which are important for the interpretation of the observations.

1.2. Instrumentation

MRO entered its Primary Science Phase (PSP) on 6 November 2006. The spacecraft is in a Sun-synchronous, roughly polar, 255 km × 320 km orbit. HiRISE provides images at spatial scales down to 0.25 m/px from this orbit and includes colour capability (McEwen et al., 2007; Delamere et al., this issue; McEwen et al., this issue). HiRISE has been used to acquire images of the martian surface at the rate of around 100 per week. The images address many different science themes. Of particular interest here is the monitoring of seasonal evolution of the southern polar region. Several sites were imaged on an irregular basis (averaging about once every 5 weeks) throughout southern spring and summer to investigate the changes in surface features as the polar regions lose their CO_2 ice coverage. In this paper, we shall describe the observations made at two specific sites informally known as "Manhattan" (99.1°E, 86.4°S) and "Inca City" (295.8°E, 81.4°S).

The planning process for MRO and the successful inter-experiment collaboration has resulted in excellent complementary and simultaneous coverage of these target sites on most observations by the Compact Reconnaissance Imaging Spectrometer for Mars (CRISM; Murchie et al., 2007) and the Context Camera Investigation (CTX; Malin et al., 2007). The combination of these data with HiRISE observations has proved to be important for the interpretation of several phenomena associated with the study regions.

2. On-set of jet-like activity

HiRISE acquired its first image of the Inca City region on 28 January 2007 (orbit 2380) with the incidence angle at 90.0°. The local time was 16:56 (see Table 1). It should be noted that the Sun at midday was already above the horizon at Inca City on the day that this first image was acquired. Despite the illumination geometry, the strong forward scattering of the atmosphere, the use of 4 × 4 binning for the image and the high signal to noise of the system led to a reasonably well exposed imaged (Fig. 1 lower left). It shows that activity (in the form of the production of dark surficial deposits) had already started. By the time of the second image on 7 March 2007 (orbit 2868), much of the field had been covered with fan deposits (Fig. 1 lower right). Within these first five weeks, activity was substantial. This rapid on-set in response to the limited solar insolation was predicted by the models of Portyankina (2006) and Kieffer (2007) and is addressed further in Portyankina et al. (this issue). Insolation may not be the sole energy source which produces this early activity. Internal heat generation (e.g. radioactive decay) and the annual thermal cycle may also play a role (e.g. Aharonson et al., 2004).

Fig. 1 appears to show that fans can develop with time – not all are the result of a single short eruption at the vent. This is not only true right at the beginning of southern spring but also later. In Fig. 2, we compare images acquired 23 days apart. Four fans are marked. At position A, the fan deposit has extended beyond a small boulder which was close to the tail-end of the fan at the time of the earlier image. The fan marked B was extremely faint but visible in the earlier frame becoming a significant feature in the later image.

Table 1
Observation log for HiRISE images used herein. CRISM ID refers to the observation identifier for a simultaneous CRISM spectral cube. Sun az. gives the azimuth of the Sun direction on non-map projected images. LST = Local solar time. The location key is as follows. Inca = Inca City (295.8°E, 81.4°S); Man = Manhattan (99.1°E, 86.4°S); Ithaca = Ithaca (181.5°E, 85.2°S).

Orbit	Date UT Time	CRISM ID	Location	Ls	Incidence angle	Emission angle	Phase angle	Scale (m/px)	Sun az. no map (deg)	LST
2380	28 January 2007 21:12:50		Inca	174.47	90.0	1.5	88.9	0.989	35.2	16:56
2868	7 March 2007 21:50:21	49A6	Inca	196.23	81.5	7.8	75.0	0.498	33.5	17:09
3092	25 March 2007 08:44:29	4F9B	Inca	206.65	76.5	1.8	78.0	0.247	32.1	16:48
3158	30 March 2007 12:09:52		Inca	209.8	76.0	2.0	73.9	0.247	32.2	16:54
3237	5 April 2007 15:53:52		Inca	213.5	74.0	4.8	77.7	0.248	32.5	16:40
3448	22 April 2007 02:28:31		Inca	223.7	70.0	4.2	73.5	0.248	33.3	16:36
3593	3 May 2007 09:38:48		Inca	230.74	67.5	6.8	73.2	0.498	35.1	16:26
3804	19 May 2007 20:14:08	5C7F	Inca	241.1	65.0	5.9	69.5	0.248	36.0	16:20
4081	10 June 2007 10:15:50	629D	Inca	254.8	62.0	0.8	62.9	0.247	38.7	16:16
4371	3 Jul 2007 00:35:38	67CA	Inca	269.1	60.0	6.5	65.2	0.248	43.1	15:50
4714	29 July 2007 18:01:49	6D64	Inca	285.8	61.0	2.0	60.2	0.248	47.2	15:50
4925	15 August 2007 04:38:08	7206	Inca	295.8	63.0	3.4	60.8	0.494	50.6	15:44
5070	26 August 2007 11:48:09	74F9	Inca	302.5	64.0	0.6	63.7	0.492	51.9	15:34
5426	23 September 2007 05:34:43		Inca	318.7	68.0	0.6	68.8	0.497	54.3	15:25
5993	6 November 2007 09:57:32		Inca	342.9	78.0	0.7	78.0	0.493	55.2	15:26
2622	16 February 2007 17:45:54		Ithaca	185.1	88.0	1.6	88.9	0.494	33.7	17:46
2675	20 February 2007 20:52:55		Ithaca	187.5	87.0	5.0	83.0	0.496	33.7	18:15
2532	9 February 2007 17:26:44		Man	181.1	88.0	27.5	110.5	0.552	37.0	16:27
2850	6 March 2007 12:08:51		Man	195.4	85.0	3.2	82.1	0.493	33.4	19:15
2942	13 March 2007 16:11:57		Man	199.6	82.0	2.3	84.4	0.491	33.4	18:41
3496	25 April 2007 20:12:45		Man	226.0	73.0	0.7	72.4	0.246	34.6	18:48
3641	7 May 2007 03:22:56		Man	233.1	71.0	0.2	70.9	0.492	36.5	18:38
5579	5 October 2007 03:41:21		Man	325.4	75.0	7.4	79.1	0.248	55.2	16:44

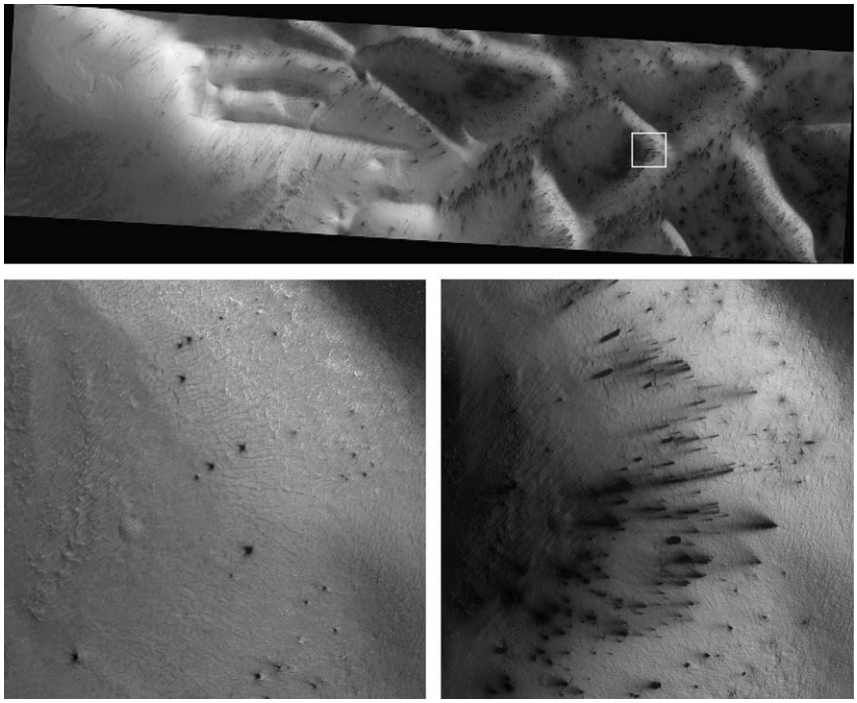

Fig. 1. A comparison between image PSP_002390_0985 (lower left) and PSP_002868_0985 (lower right) taken 37 Sols later (Ls = 174° and 196°, respectively, LSTs = 16:56 and 17:09, respectively). The position of the sub-images is shown on the larger scale image at the top by the superimposed rectangle. The sub-images are of an area of 800 m × 800 m. A significant amount of fan activity has occurred between the times of the two images. Note also that the orientations of the fans on the right follow the local slope. Fans at the bottom of the image are roughly horizontal, fans at the top of the image point towards the lower left. This is an indication of topographic control of fan direction. Observational conditions for these images (and for all other images presented) are given in Table 1. These data have been geometrically rectified so that the solar azimuth is 128°.

The fans marked C and D are similar but less extreme examples of continuing and repeated activity. There are numerous other examples of this phenomenon throughout the Inca City region.

There are at least six possible explanations for observations of continuing or repeated activity. First, the vent may reseal itself by some process which is not known. In doing so however, this resealing process cannot act to strengthen the ice sheet to such an extent that the vent is no longer the weakest point in the local ice sheet. Otherwise venting from this source would not restart. Second, outgassing may occur episodically when

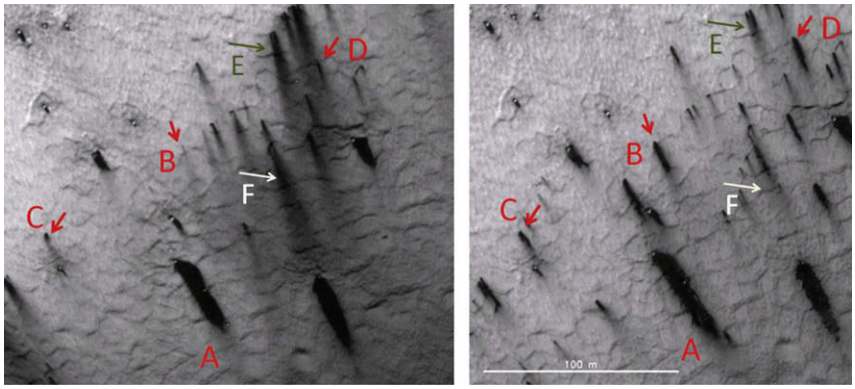

Fig. 2. Comparison between images PSP_002868_0985 (left, Ls = 196°, LST = 17:09) and PSP_003158_0985 (right, Ls = 210°, LST = 16:54). Six fans are marked. It can be seen that between the acquisitions of the two images, the fan deposit marked A has extended beyond a boulder which was close to the apex of the fan at the time of the earlier image. The fan marked B was extremely faint but visible in the earlier frame becoming a significant feature in the later image. The fans marked C and D are similar but less extreme examples of continuing activity. The fans marked E and F appeared to be larger and darker in the earlier image. This may be evidence for activity in progress at the time of the acquisition of the first image.

individual channels under the slab ice become open (through additional sublimation) and the transporting gas is free to reach a permanently open vent. Third, the insolation and gas production may be strong enough to produce eruptions on a diurnal cycle so that outgassing and dust deposition is a daily process until all CO_2 ice has been used up. It is important here to recognise that the latter is not an explosive process preceded by pressure build-up. Fourth, there could be superposition of two or more vents in close proximity such that it becomes impossible to distinguish the individual sources even at HiRISE resolutions. There would however be a requirement here to tap different gas pockets in very close proximity. Fifth, as the slab ice thins the albedo may decrease leading to enhanced energy absorption which further fuels sublimation from the base. Finally, the CO_2 ice slab might be lifted by the pressure underneath to initiate activity. Once the pressure is released the slab slumps back to the surface and the process repeats. Combinations of any these mechanisms are also possible.

There is additional evidence that activity may be sporadic at some sites with varying degrees of activity. In Fig. 3, two "classical" fan deposits on a relatively flat surface can be seen emanating from and surrounding araneiform surface structures. The large deposit to the left appears relatively uniform in appearance. However, an image acquired several weeks later (Fig. 4) shows the same deposit but at its centre, the deposit is distinctly darker. This deposit is much smaller, almost circular and roughly centred on the araneiform structure. This type of surface deposition is common in Manhattan.

Observations have also been obtained of changes similar to those in Fig. 2 but on very short timescales. Fig. 5 shows a region in a part of the cryptic terrain known informally as "Ithaca" (181.5°E, 85.2°S). Here there are no spiders and a lacertilian surface texture (Hansen et al., this issue). These two images were taken just 106 h apart. Fans appear to emerge from point sources rather than elongated cracks and are seen to lengthen in the time between the images. Fans from a single point go in multiple directions, possibly reflecting changes in direction of the local wind or a changed vent geometry. Bright fans are observed, which are frost rather than dust. Spectroscopic data from MRO's CRISM instrument indicate that these bright fans are composed of CO_2 frost (Titus et al., 2007). Conditions for formation and retention of the bright fans must be limited, because these particular bright fans were not observed again after Ls = 187° at the Ithaca site.

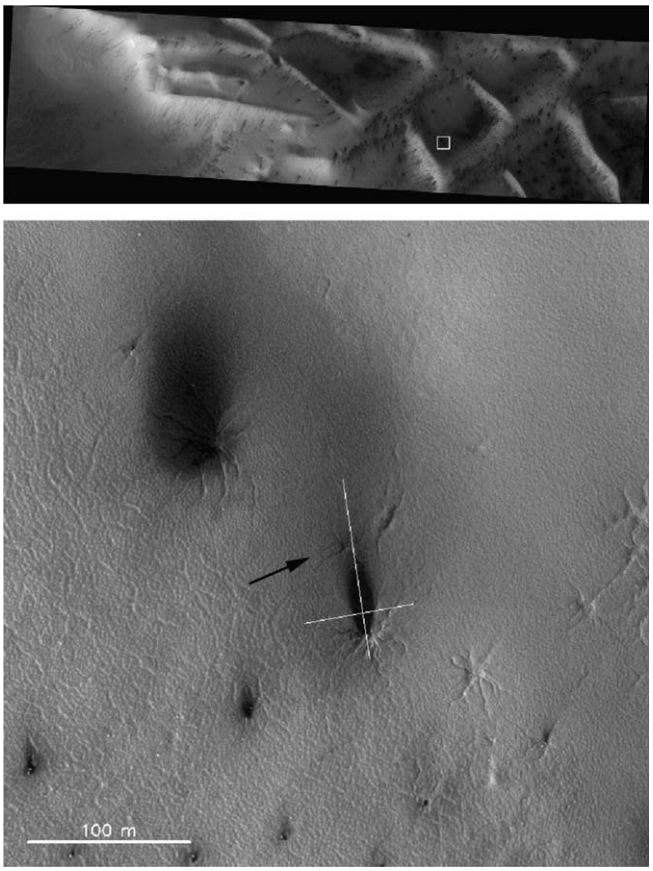

Fig. 3. Emission from araneiform structures in a relatively flat area in the Inca City region (image PSP_002868_0985). The image shows classical fan-like deposition patterns which provide a uniform coverage of the surface when compared to deposition patterns on slopes. Several other spider structures in the field became active later in the season. The black arrow points to one specific example discussed in the text. Lines show locations of profiles in Fig. 8. This image has been geometrically rectified. The solar azimuth is 128°.

3. Evidence for freezing-out of jet-driving volatiles

When viewed in enhanced colour (Delamere et al., this issue), HiRISE data show that the dark jet deposits appear in many places to be surrounded by slightly brighter, bluer deposits (Fig. 6).

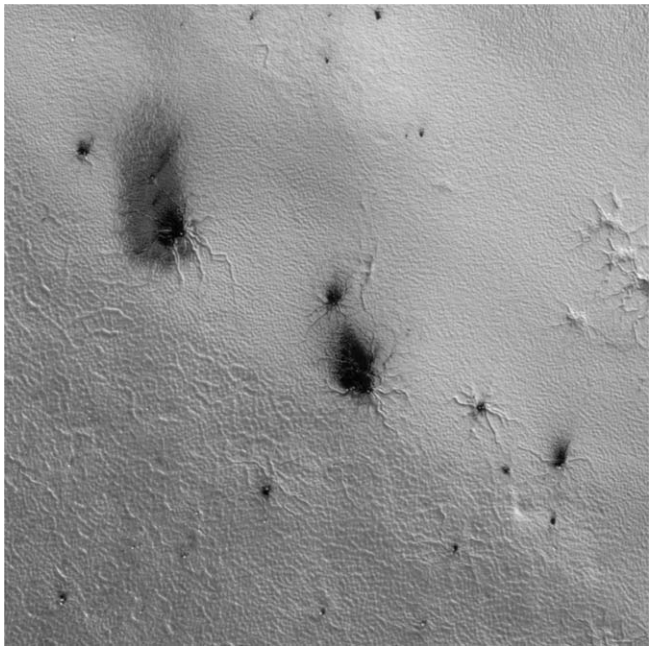

Fig. 4. Section of image PSP_003593_0985 (Ls = 231°, LST = 16:26). Note in particular the large fan deposit to the upper left. Around the presumed source of the emission (near the centre of the araneiform surface structure), a darker deposit appears to be superposed on a lighter deposit. This should be compared with Fig. 3 which shows the same region several weeks earlier. In that image, there is no evidence for such an inhomogeneous deposit structure.

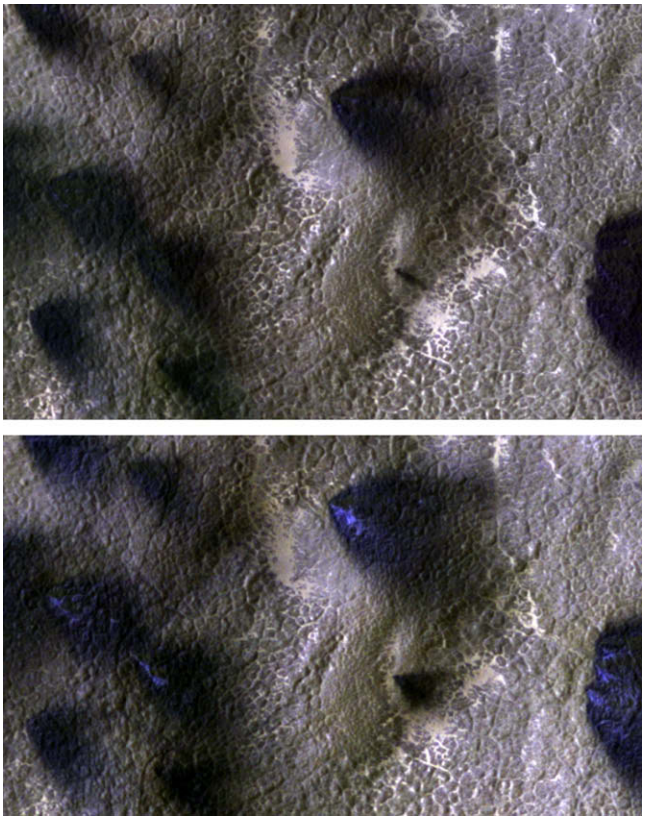

Fig. 5. Ithaca images PSP_002622_0945 (top, Ls = 185°, LST = 17:46) and PSP_002675_0945 (bottom, Ls = 187°, LST = 18:15), acquired 106 h apart, in false color emphasise changes in the color, morphology, and extent of the fans.

Following Titus et al. (2007, 2008), we interpret these brighter deposits as the result of condensation of a volatile brought to the surface by the jet with the most likely candidate for the volatile being CO_2. These deposits become clearly evident when a colour ratio is made between the HiRISE blue–green and red channels. The increased reflectivity in the blue probably arises from the CO_2 ice deposit being fine-grained and relatively opaque thereby obscuring the redder surface beneath. The redness of the original surface may be produced by a thin dust or fines covering on the slab ice, it may be influenced by the red surface below an almost completely transparent slab ice layer, or it may be residual fines within the slab deposited at the same time as the slab itself.

Occasionally, the brighter material appears with only a faint or indeed non-existent dark deposit. There is no obvious reason why outgassing must be accompanied by the appearance of a dark deposit. One could envisage a pure gas jet if the substrate is sufficiently consolidated so that no particles can be entrained in gas transport. In analogy with a similar concept on Io (Johnson et al., 1995) one could refer to these as "stealth jets".

There are two possible mechanisms for producing the bright deposits. At the vent, the CO_2 is under pressure and expands. This results in a rapid cooling (which may or may not be fully adiabatic depending upon the dust particle density and its thermal coupling to the gas and the coupling between the ambient gas and jet gas) as it leaves the vent. If the gas is cold relative to the ambient gas through expansion, then condensation can occur followed by fallout. Alternatively, the gas pressure may be raised locally so that it exceeds the equilibrium vapour pressure at the ambient temperature. In other words, it is not clear whether locally low temperature or locally high pressure leads to the condensation and detailed modelling (taking into account the dust particles and the ambient gas as potential heat sources) is required.

4. Evidence for jet-like activity during a HiRISE observation

The observation of jet-like activity in progress has been a high priority goal for the HiRISE Science Team. It is clear that with the level of activity seen within the Inca City, Manhattan, and Ithaca regions, it would be perhaps surprising if activity at some level had not been occurring during the observing campaign.

Several attempts have been made to detect the existence of ongoing activity. The primary goal of such attempts has been to quantify the heights and widths of the jets and to assess their dust content (through measurements of the opacity with height). Our preferred approach has been to obtain stereo observations of candidate sites as rapidly as possible. The optimum that can be achieved is a sequence of three images on consecutive orbits. The first two images are acquired on consecutive orbits using the ascending section of the orbit (Graf et al., 2005). The third can be obtained on the following orbit by taking advantage of the site's high southern latitude to obtain an observation on the descending part of the orbit. (This is one of the few occasions when HiRISE has observed on the descending part of the orbit.) Through this complex observing plan, three images of the site can be obtained within 5 h.

Despite several attempts with this method, no unambiguous evidence of a plume has yet been obtained. There are several possible explanations for this null result. First, activity may be concentrated in the morning and midday hours – all HiRISE observations of the Inca City sites were obtained in mid- to late afternoon (see Table 1) because of the Sun-synchronous orbit. Second, the plume height may be rather small. Although Kieffer (2007) computed a possible plume height of up to 1 km, this is clearly an upper limit and adjustment of parameters can lead to much smaller estimates. We will show below that heights well below 100 m are consistent with the appearance of the majority of fan deposits in Inca City and that many deposits may be the result of ground-hugging flows rather than emission plumes. Third, it is possible that the plumes

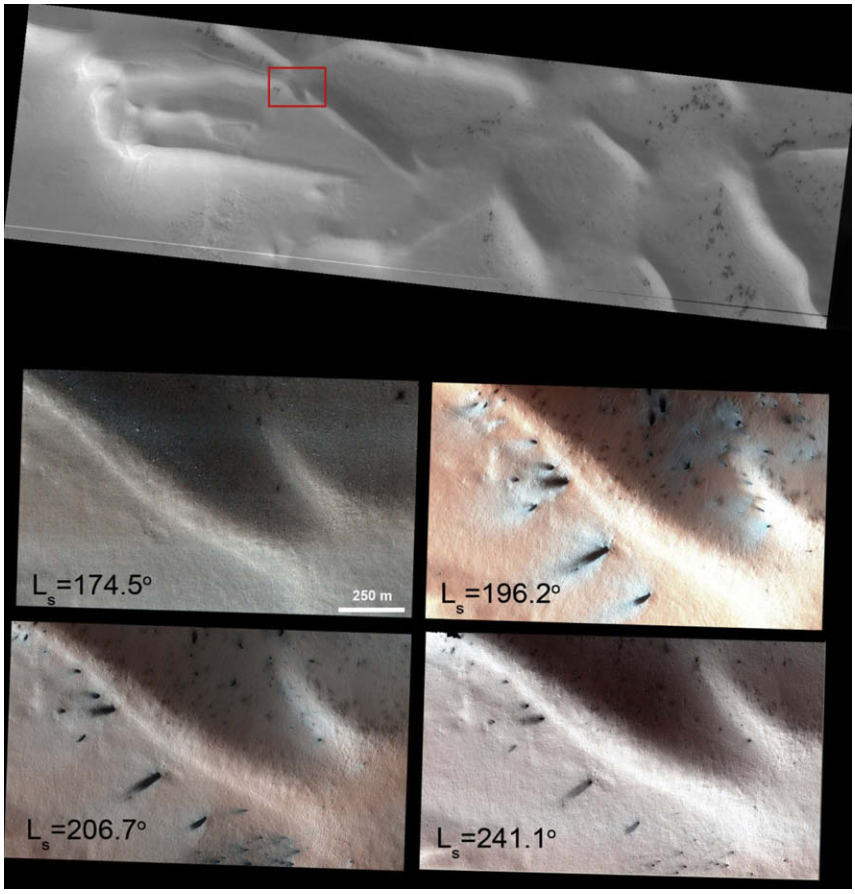

Fig. 6. Time series of the region indicated in the top image by the red box. Centre left: PSP_002380_0985. Centre right: PSP_002868_0985. Bottom left: PSP_003092_0985. Bottom right: PSP_003804_0985. The series shows that using enhanced colour, the dark deposits appear to be surrounded by brighter, relatively bluer deposits which may be the result of the freezing out of CO_2 which is coming out of the vent. The images have been geometrically rectified and individually contrast enhanced.

are optically thin because of relatively low dust content and are simply invisible at optical wavelengths. Despite the lack of success, further attempts will be made in the coming season and alternative strategies will be attempted.

In the absence of evidence from stereo observations, the key question is whether activity can be recognised as such in individual images. In Fig. 2, there are two areas (marked E and F) which appear darker in the earlier image (PSP_002868_0985) and which show, in the later image (PSP_003158_0985), a dark deposit that is much smaller than might be inferred on the basis of the earlier image alone. A possible explanation for this phenomenon is that the sources were actively emitting at the time the earlier image was acquired. The flow here is downhill and one might assume that cold gas transports the dust down to the base of the slope where it is deposited leaving only part of the slope itself covered by a deposit. In the Inca City region, the bases of the slopes where activity is occurring are covered with diffuse dark material relatively early in the spring season (see for example, Fig. 1 top and lower right).

Three further examples of possible plumes are shown in Fig. 7. This shows a time sequence covering images PSP_002868_0985, PSP_003092_0985 and PSP_003158_0985 – a total duration of 23 days. The arrows indicate three sites on the images. At all of these sites, the earliest image shows an extended and somewhat diffuse fan which is not seen in the two later images. Other features common to the three images do not appear to have evolved in a similar manner. Several features are identical in all three images, while others have appeared or grown over the 23 day duration.

We shall see in the next section that topography appears to influence the deposition pattern on the surface in several places. This is evident in the large dark deposit roughly in the centre of the frames in Fig. 7, for example. The three possible plumes in Fig. 7 show no obvious evidence of inhomogeneous coverage. There are no abrupt, sharp diversions in the shape and uniformity of the margins of the supposed plume. The margins are very diffuse, uniform, and independent of the surface relief. This is fully consistent with the idea that these dark particles are airborne.

If one assumes that the marked features in Fig. 7 (left) are deposits on the surface then it is not obvious how one can "clean" the surface in such a way as to remove the dark material so that just 18 days later (Fig. 7 centre) the surface appears similar to the surrounding bright areas and the fan deposit appears to be much shorter. If one invokes an aeolian process, it is necessary to explain why other fans have not been affected and why there are no residual trails or streaks. A darkening of the entire bright surface to reduce contrast can be ruled out (see Fig. 18 later). If it is assumed that the marked features in Fig. 7 (left) are indeed actively emitting at the time of imaging, then it follows that activity can occur late in the day because the image in Fig. 7 (left) was acquired at a local solar time of 17:09 (see Table 1).

5. Activity sources and evidence for topographic control of deposition patterns

5.1. Spiders

Araneiform structures are a source of fan-like deposits within the Inca City study area. Two examples are seen in Fig. 3 which

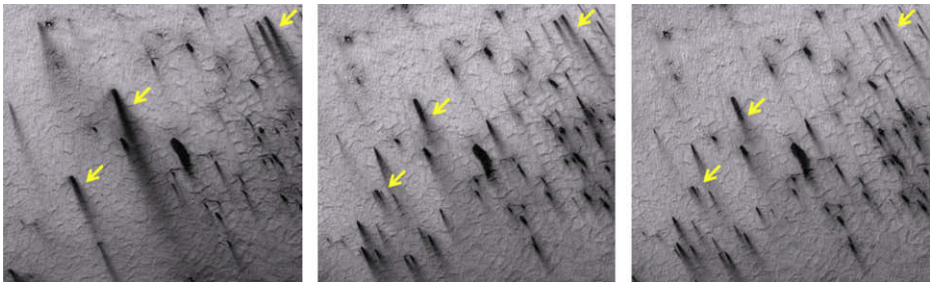

Fig. 7. From left to right. Images PSP_002868_0985 (Ls = 196°, LST = 17:09), PSP_003092_0985 (Ls = 207°, LST = 16:48), PSP_003158_0985 (Ls = 210°, LST = 16:54). The image acquired on orbit 2868 shows three very extended fans (marked by the arrows) which are only apparent as shorter length deposits in the other two images. However, additional deposition fans (which presumably indicate activity break-out after acquisition of the previous image) are evident in both images to the right. The sub-images show a region 400 m × 400 m in area.

is taken from image PSP_002868_0985. These structures form the "classic" case as described by Piqueux et al. (2003). The reflectance of the dark deposits is typically 20–40% of the surroundings early in the spring season. Fig. 8 shows profiles across one of the fan deposits. The profile perpendicular to the direction of flow indicates a full-cone angle for the deposit of between 40° and 45°. Along the long axis of the deposit, one can see that for the first 40 m from the inferred source, the reflectance is constant suggesting complete surface coverage out to this distance. The reflectance then rises to reach the background surface level about 80 m from the inferred source.

Five weeks earlier (in image PSP_002380_0985) the dark deposit was considerably smaller and roughly circular (and similar to the spots seen in Fig. 1 left). This suggests either gradual pressure release or multiple events. In Fig. 3, there is an araneiform structure with no associated dark deposit at the end of the deposit described in Fig. 8. This structure became active within the following 18 Earth days to produce a dark deposit (Fig. 4). Finally, the second major source in Fig. 3 showed no deposition pattern in image PSP_002380_0985 and was therefore presumably inactive at this earlier time. Hence, in this small area, araneiform structures separated by at most 150 m on relatively flat terrain initiated fan deposition at different times.

Some spiders within the Inca City monitoring area showed no activity at all during this season while others were rather weak

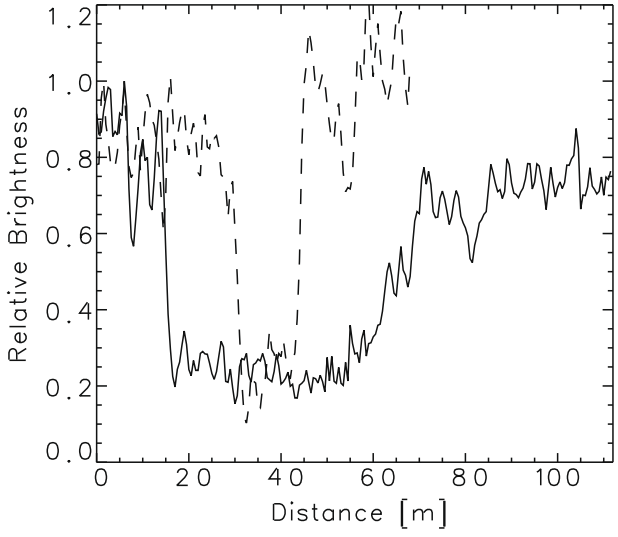

Fig. 8. Profiles through the fan deposit shown in Fig. 3. The solid line gives the relative reflectance from bottom to top along the symmetry axis of the fan. The dashed line gives the reflectance perpendicular to the axis around 13 m from the inferred source.

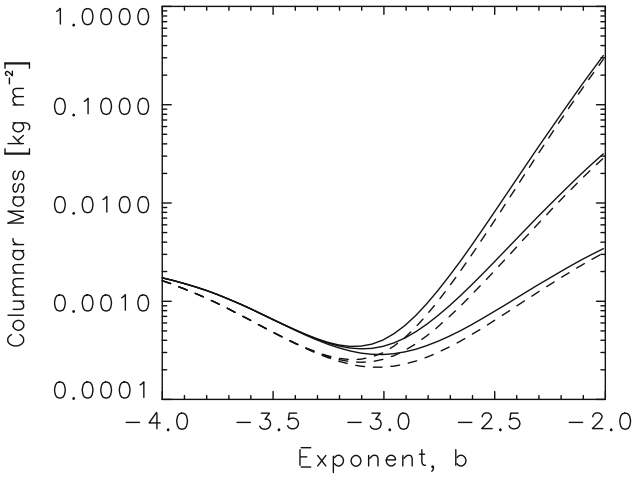

Fig. 9. The columnar mass of particles in a plume for different values of the exponent of a power law. An exponent of −4 corresponds to a mass distribution dominated by small particles, an exponent of −2 corresponds to the mass being dominated by large particles. The solid lines are for a refractive index, $n = (1.50, 0.01)$, the dashed lines are for $n = (1.70, 0.01)$. The pair of lines with higher columnar masses at larger exponents has been produced using a largest transportable particle radius of 1 cm. For the middle pair the largest transportable particle radius was set to 1 mm and for the lower pair 0.1 mm.

(Fig. 10 left) and hence the mere existence of a spider is not a guarantee of activity. Many spiders show dark deposits emanating from the edges of their central depression (Fig. 10 right). This suggests a mechanism for enlarging the central depression. The ice slab drapes over the spider but may be weak at the lip of the depression. Venting activity therefore initiates at the lip and erosion of the lip occurs through local gas and dust transport. In this way, spiders grow outwards through erosion of the walls.

Other examples of araneiform structures are given in Hansen et al. (this issue).

5.2. Cracks on slopes and evidence for near-surface flow

In the Inca City region, araneiform structures are restricted to slopes of low inclination (see below). However, fan deposits are clearly evident on the sides of steeper slopes where no spiders exist. Spots associated with no evident spider structure but with cracks, some of which are roughly orthogonal to the direction of the local surface slope, are also producing fans (see Figs. 1 and 2. There are other examples throughout the region). Emitting cracks are in very close proximity to each other. If the outgassing mechanism of Kieffer et al. (2000), Kieffer et al. (2006), and Kieffer (2007) is correct then the sub-surface source region for this activity must

be considerably smaller than is widely assumed for the spiders and yet the degree of activity appears to be comparable. Initiation here may be the result of gravitational stresses on the slab ice producing cracks above or close to local topographic features.

In Fig. 1, the fan deposits resulting from the gas jet activity are typically 100 m long (some lengthen through the season). The dark deposits expand from the inferred vents to produce roughly conical deposits with full-cone-angles of about 15–25° and hence somewhat less than observed on flat ground.

On the lower right of Fig. 1 the direction of the downward slope changes considerably. One can see that the fan deposits arising from jet activity change their direction in response to the local slope. In this case, the MOLA topographic map indicates the approximate magnitude and direction of the local slope and hence this is unambiguous. In addition, in regions with rapidly changing slopes, in which we must infer the local slope because of the lack of high resolution topographic data, the deposits also appear to follow the local slopes. This does not exclude the possibility of local catabatic winds influencing particle motion. It merely says that large scale wind phenomena are not the dominant force shaping the fan deposits in this particular region in this particular year.

On relatively flat surfaces, the fan deposits are quite uniform in appearance (Fig. 3). On the other hand, at the highest resolution, the deposits on the slopes frequently do not provide a homogeneous coating (Fig. 11). Neither do the fan deposits provide a smoothly varying coverage which reduces monotonically with distance from the vent. Instead, many deposits are patchy and appear to be influenced by small scale topographic features on the surface. We consider this to be strong evidence that particle transport in the flow is close to the surface. It is difficult to envisage this as being the result of airfall from altitudes of 50 m or higher. The ballistic and gas drag calculations given below also indicate that

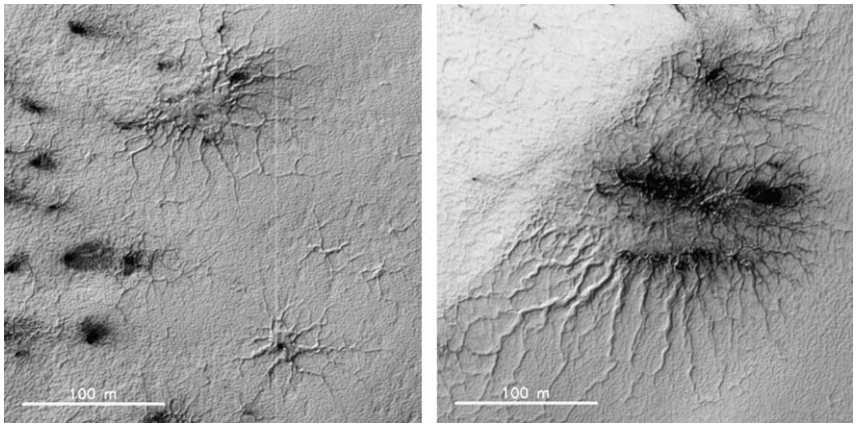

Fig. 10. Two sub-images of PSP_003593_0985 (Inca City, Ls = 231°, LST = 16:26). On the left, we see two relatively small spiders. The upper spider shows only weak evidence of activity. The lower spider showed no evidence of activity even at this relatively late stage in the season. On the right, we see a larger spider structure which seems to be active around the boundaries of the central depression. This suggests that the spider grows radially because of erosion of its perimeter.

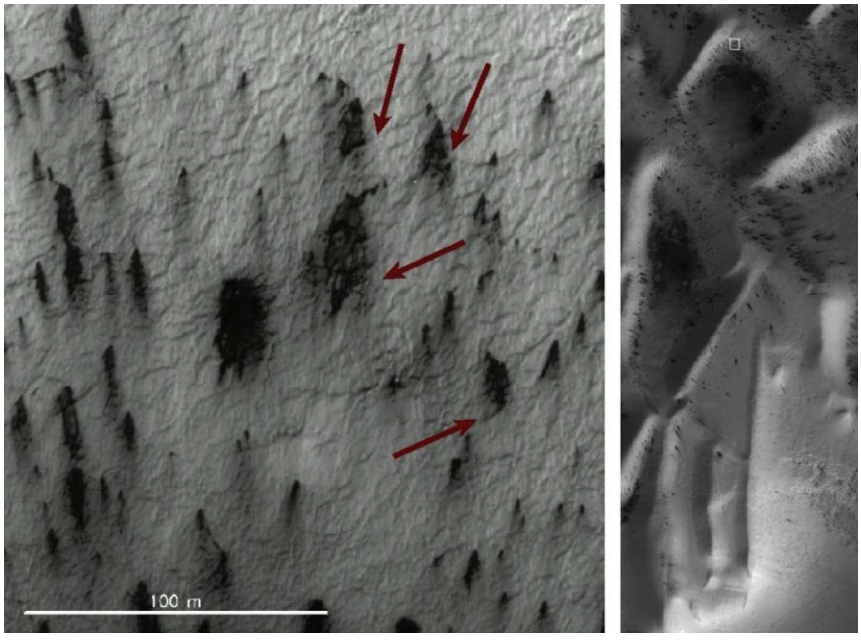

Fig. 11. Image PSP_003158_0985 (Ls = 210°, LST = 16:54) shows evidence of transport very close to the surface. The deposition pattern is influenced by the small scale topography on the surface itself. Good examples are indicated by the arrows. The full-frame image to the right is around 5 km across. The small box at the top of this image indicates the position of the sub-frame shown on the left.

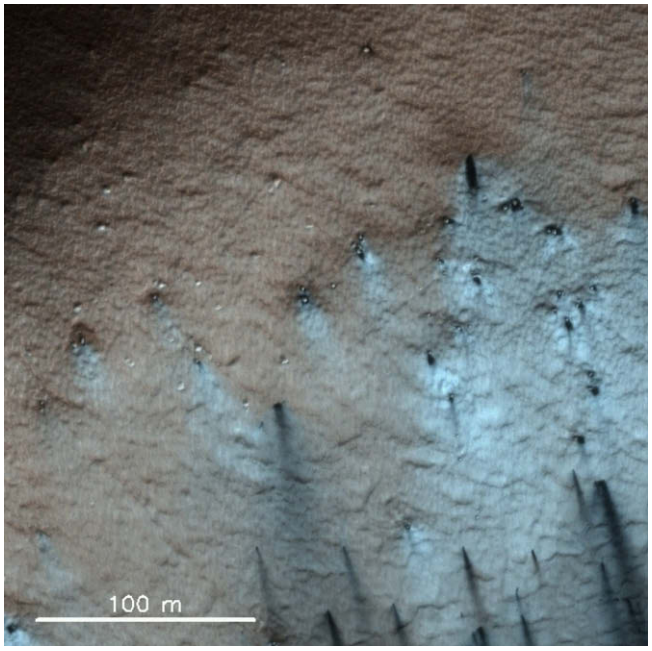

Fig. 12. Image PSP_002868_0985 (Ls = 196°, LST = 17:09) shows a series of rocks or boulders on a ridge. They are often surrounded by dark material and sometimes appear to be the sources of dark material. This colour representation also shows brighter bluer deposits apparently originating at boulders suggesting that CO_2 outgassing is occurring.

ejection from the vent is of such low velocity that topography can influence the deposition pattern. We envisage this outgassing as being similar to fumaroles in volcanically active regions on Earth. On Mars, however, the outgassing is of cryogenic origin and hence they might be described as "cryo-fumaroles".

In this interpretation, the gas is ejected from the vent at a very low ejection velocity but at sufficient densities to entrain dust particles and at densities somewhat higher than the ambient CO_2 density. As the gas expands from the vent, it cools and becomes colder than the surrounding ambient gas. The cold vent gas is heavier than the ambient gas and therefore sinks to lower elevation, i.e. it moves downhill. (This supplements the behaviour expected if the vent axis is perpendicular to the local slope as described for large particles by the ballistic calculation below.) As the cold gas drifts downhill, it meets local topographic maxima which are sufficient to slow the gas whereupon it releases some of its dust particles to produce a patchy deposition pattern. On relatively flat surfaces, this does not occur but deposition occurs when the particles fall out under the influence of gravity and gas drag, thereby leading to a more uniform deposition pattern.

5.4. Boulders

The ridges of Inca City appear to have a small but significant number of boulders on them. These rocks are often surrounded by dark material which appears to be similar to that contained within the fan deposits (Fig. 12). These darker rings were evident very early in the season (e.g. image PSP_002868_0985). It is conceivable that rocks retain heat input during summer because of their high thermal inertia. This heat is released during winter to reduce the CO_2 frost deposition and hence it is cleared of CO_2 earlier in the spring than other areas. This hypothesis needs to be tested however. In particular, it should be noted that the rocks are close to or smaller than the annual thermal skin depth (about 1 m; e.g. Kieffer, 2007) and hence heat retention to prevent condensation is likely to be marginal. The draping of the CO_2 slab ice over the boulders and the resulting irregular structure of the slab may here again play a role in defining when and where activity initiates.

5.5. Quasi-linear sources on flattish ground

In areas of flattish ground, quasi-linear deposits of dark material can be seen in images in the early part of southern spring. A typical example is shown in Fig. 13. The left side of the figure was taken from image PSP_002868_0985 and shows several features. There are inactive spiders to the top right of the image (which do not appear to have become active at all during this martian year), there is a circular deposit which one presumes has a jet-like source, and there are quasi-linear features which seem to have associated dark deposits. These deposits are not uniform along the linear structure but appear at irregular intervals separated by distances just greater than the resolution limit thereby giving the impression at first sight of a discontinuous fissure-type source. The quasi-linear deposits appear to cross each other but there is no regular pattern. Later in the season, several fan-like deposits appear (seen clearly in image PSP_003593_0985) and the surface of the whole region becomes increasing covered in dark material but the quasi-linear sources remain visible although they do not seem have grown with time as fan deposits usually do.

At the end of the season (see Fig. 13 right), once the CO_2 ice has sublimed, there is no obvious surface feature which can be related to the activity seen earlier in the season. There appears to be surface roughness but there is little or no indication of why one point should become active and another not.

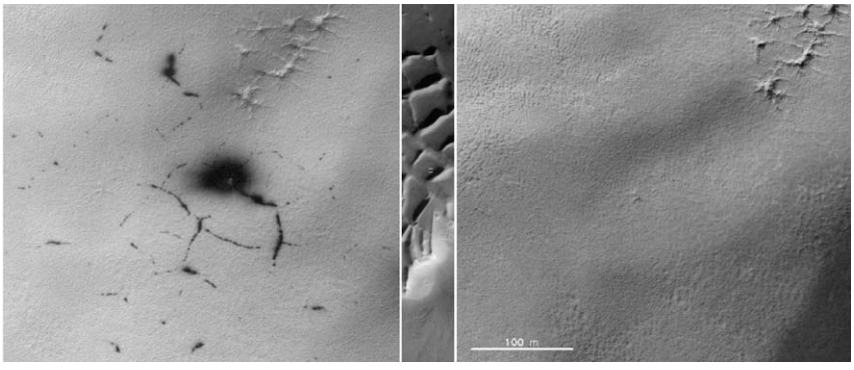

Fig. 13. Left: Sub-image from PSP_002868_0985 showing dark deposits on the surface in quasi-linear structures which might be interpreted as cracks. Centre: the position of the sub-image is shown as a small box within the full-frame image PSP_005993_0985 (which is roughly 5 km across). Right: the same region as seen in PSP_005993_0985 (Ls = 343°, 15:26). This shows no obvious structural relationship between the terrain after CO_2 sublimation has completed and the positions of the quasi-linear structures.

This type of behaviour may be the result of pressure under the CO_2 slab forcing the slab upwards and producing a linear rupture or crack with subsequent ejection of material. This can only occur in relatively flat regions where there are no local areas of weakness.

6. Simple models of surface deposits and outgassing

The modelling of a dusty gas jet on Mars is less straightforward than a corresponding model for, for example, Triton (Kirk et al., 1995) because of the thickness of the ambient CO_2 atmosphere which necessitates a detailed fluid dynamics calculation. In particular, the dust particle size distribution and its effects on the mass loading of the outflow from the vent are difficult to model and constrain. However, we can use simple models to estimate properties of the jets in a way that leads to some simple constraints on basic parameters.

The observables that can be used to provide these constraints are the lengths and angular widths of the fan deposits (typically >80 m and ≈35° full-cone, respectively) and the surface slope which, for Inca City, has been deduced from the MOLA data albeit at much lower resolution and is taken to be around 20° for the slopes seen in, for example, Fig. 1.

6.1. Ballistic calculation

We first use a ballistic approximation to match the deposition patterns and thereby estimate ejection velocities. This assumes that particles are large to the point that gas drag, after leaving the vent, is negligible at both ambient pressures and pressures within the outflow. Using the drag equation, the atmospheric density, and the Mars gravitational force, one can estimate that for particle sizes of around 150 μm, the drag force in the ambient atmosphere for velocities around 10 m s^{-1} is about ¼ of the gravitational force and hence a ballistic calculation for particles of this size and larger is not unreasonable.

A ballistic model has the advantage of being trivial to construct (see for example Strom and Schneider (1982)) and can easily be adapted to include the orientation of the local slope. A typical result is shown in Fig. 14. The observables can be re-produced using an ejection velocity of 15 m s^{-1} and a full-cone angle for the emission at the vent of 6°. The result is a reasonable approximation for some of the more homogeneous deposits seen on slopes. Small changes in the parameters also lead to results consistent with some observed fans. In most cases, the ejection velocities reproducing the observations are in the range 10–20 m s^{-1} with a rather narrow angular ejection profile (<6° full cone). This results in a typical height above the surface of around 100 m for the peak of the ejection plume and therefore considerably smaller than the 8 km high plumes on Triton (Kirk et al., 1995) which may be produced by a similar process.

6.2. Gas drag calculation

Another simple model to construct is to assume that particles are ejected perpendicular to the local surface to a specified height. Then, under the influence of gravity, they fall back to the surface but with the additional opposing influence of gas drag. Wind can now be introduced consistently as an additional free parameter. We follow the approach given by Kieffer (2007) who computed fall times for different particle sizes from 1 km altitude.

Here we use the observables again (the length of the fan deposits and the magnitude of the surface slope) together with an estimate for the particle size to determine the initial height of the particle as a function of local wind speed. The typical particle size in this area has been derived from thermal inertia measurements (Paige and Keegan, 1994) to be between 100 and 200 μm. We choose here 150 μm radius for our calculations.

With these parameters, it is again found that even for relatively low wind velocities (≈1 m s^{-1}), the heights of the jets are 60 m at most (Fig. 15). Only in the case where the local wind velocity is 0 m s^{-1}, do estimated jet heights come close to the upper limit determined by Kieffer (2007). For smaller particles, the sinking time is longer and hence local wind velocities are even further limited by the deposition pattern.

Hence, the two approaches considered here, (the ballistically dominated ejection and the falling time calculation) suggest plume heights between 50 and 100 m are the maximum necessary to produce the observed deposition patterns. These maximum values

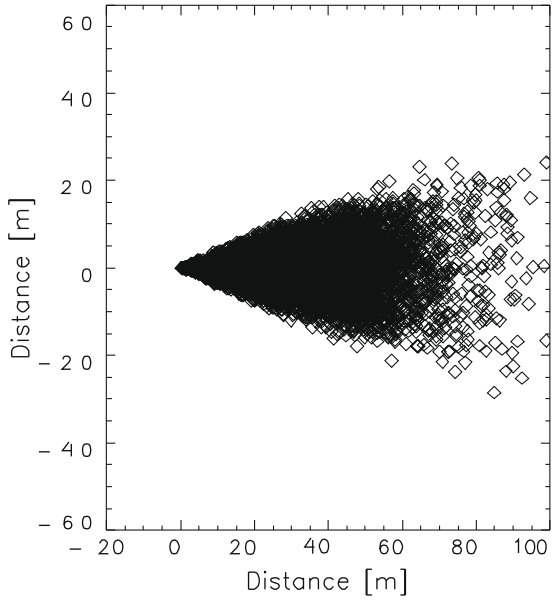

Fig. 14. Result of a ballistic calculation for a jet-like plume of large particles. The surface tilt used was 20°, emission velocity was 15 m s^{-1} with a standard deviation of 5 m s^{-1}, the spread at the vent was set at ±3°. Emission was normal to the surface. The fan extends downslope.

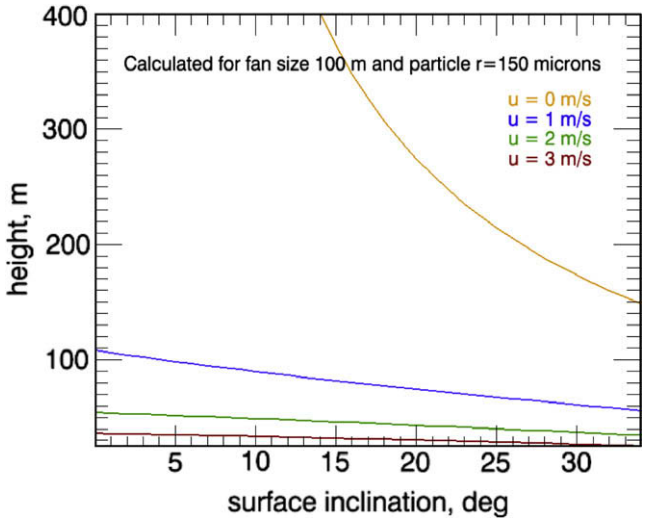

Fig. 15. Height of jet required to produce 100 m long fan deposits for a range of surface inclinations and wind velocities. The calculation assumes fall out of 150 μm radius particles under the influence of gravity but opposed by gas drag. Note how low the maximum altitude of the jet must be for the slopes seen at Inca City.

should result in plumes visible and quantifiable in HiRISE stereo imagery of the sites. The fact that at this time, no unambiguous detection of plumes through stereo imagery has been made suggests that even these plume heights might not be achieved. We consider that many observed deposition patterns on slopes could be explained by heights an order of magnitude lower.

6.3. Plume mass ejection rates

One can attempt to place constraints on the mass loss of particulate material from the jet although this depends rather strongly on parameters which can only be weakly constrained themselves.

Plotting along the axis of one of the inferred plumes in Fig. 7 towards the source shows that one never reaches an optically thick state (where the observed intensity is constant). However, the intensity of the inferred plume does come close to that of surrounding fan deposits which we assume to be dormant and obscuring the ice below. Hence one can infer that the optical depth is likely to be about one. Taking a particle size distribution in the form of a power law, i.e.

$$N(r) \propto r^b$$

one can compute the cross-sectional area of the particles in the distribution to produce an optical depth of one and hence deduce the mass in a column to the surface assuming a density. The computation can be improved by using Mie theory (Bohren and Huffman, 1998) to estimate the optical cross-sectional area if the particle refractive index, n, can be constrained.

In Fig. 9, the result of an example calculation is shown. For a range of values of b, the optical cross-section (extinction cross-section) required to produce an optical depth of one has been computed. This has been converted to a mass using a particle bulk density of 1500 kg m^{-3}. Calculations for two different values of n are shown although this has relatively little influence on the result. These values can be compared with those found in astronomical databases (Henning et al., 1999) for specific materials (e.g. pyroxene). A wavelength of 600 nm has been used.

The range of b considered encompasses a wide range of possibilities. If $b = -3$, each particle size contributes equally to the total mass. Hence, the cross-sectional area of the particles decreases linearly with increasing size. If $b = -2$, the larger particle sizes dominate the mass. In both cases (and particularly for the latter), it is necessary to incorporate a cut-off size which expresses the largest particle size allowed in the distribution. This has been set to 1 mm (lower pair of lines) and 1 cm (upper pair of lines). It can be seen that this cut-off changes the result significantly for exponents, $b > -3$. A minimum can be seen at about $b = -3.1$ which comes about because, with smaller exponents, the number of smaller particles rises but these have a much lower optical efficiency and hence the total mass has to increase to get enough optical active particles to meet the criterion of unit optical depth. This leads to the minimum columnar mass in the plumes being $>3 \times 10^{-4}$ kg m^{-2}.

The plumes in Fig. 7 (left) are around 10 m across but the flow rate downhill is extremely uncertain. We are currently performing a series of fluid dynamics calculations in preparation for further publications. These initial studies indicate that flow velocities of the order of 10 m s^{-1} are to be expected. This leads to an estimated minimum production rate of 30 g s^{-1} for the particulate material.

6.4. Outgassing duration

Modelling work (Kieffer, 2007) assumes that a quantity of gas can be trapped and then rapidly released through a rupture. The pressure of gas trapped might be equal to the overburden pressure of 30–50 cm of seasonal ice (Kieffer, 2007). As the Sun rises, the pressure increases and hence rupture would be favoured in the mornings or around midday. It is possible to estimate the duration of activity. Let us assume that the seasonal average sublimation rate is 10 kg m^{-2} day^{-1} (Kieffer, 2007). Assuming the mass of the gas trapped is the result of 5 days of sublimation at this rate, application of Bernoulli's theorem gives the velocity and flux of the gas, as a function of the area of the orifice through which the gas escapes. The two equations required to compute eruption duration are:

$$v = \sqrt{\frac{2p}{\rho}}$$

and

$$t = \frac{M}{\rho A v}$$

where v is the velocity, p is the gas pressure, ρ is the gas density, M is the mass of gas to expand, A is the area of the orifice, and t is the evacuation time. The gas pressure can be set to be equal to the overburden of ice above the gas. For typical ranges of the other parameters, t = 10 min to 2 h. Hence, it is difficult to reconcile late afternoon emission with midday (or morning) initiation given these durations. The only means to accommodate late afternoon emission is to have very large (several hundred metre in radius) reservoirs or extremely narrow orifices.

However, we know very little about the rupture process. For example, repeated emissions from the same source are not easily explained as noted above. Furthermore, there are other mechanisms that might play a role. Dust particles on the surface sink through the ice layer rather effectively even at larger solar zenith angles. This may create the weakness necessary for activity later in the day. Expansion or cracking of ice under thermal flexure may also be involved. The observations we show in Fig. 2 are of a steep slope so that gravitational effects may also be significant as an initiation process. In any event, the conclusion must be that initiation is a complex process which strongly depends upon the local conditions and that conceptually a combination of circumstances can be arranged such that jet activity in the late afternoon can occur.

7. Yearly surface evolution

7.1. Spider evolution

Fig. 16 tracks the evolution of a spider in the Manhattan region through spring, starting at Ls = 181°, just after this latitude began to be illuminated. Study of numerous araneiform and other channel morphologies in HiRISE images suggests the following annual cycle: (1) Dust ejected out of an opening in the seasonal ice layer settles on top of the translucent seasonal ice on the surface. The vent size ranges from small depressions accessing the subsurface to lengthier openings along a channel side. (2) The dust is transported across the surface – and probably close to the surface, getting preferentially trapped in the channels. It is seen to drape around small-scale undulations of the surface. We assume that the dust remains only weakly consolidated over the yearly cycle. (3) Seasonal ice sublimes completely, and channels carved in the substrate are still visible but fans blend back in with the surface material. (4) The next winter seasonal CO_2 coats the ground relatively evenly, conformally coating the surface. (5) In channels however the underlying dust is more permeable than underlying hard ice-cemented ground, which facilitates gas transport in the same place year after year. (6) Channels grow as CO_2 gas flows through and entrains material from the sides and floor of the channel year

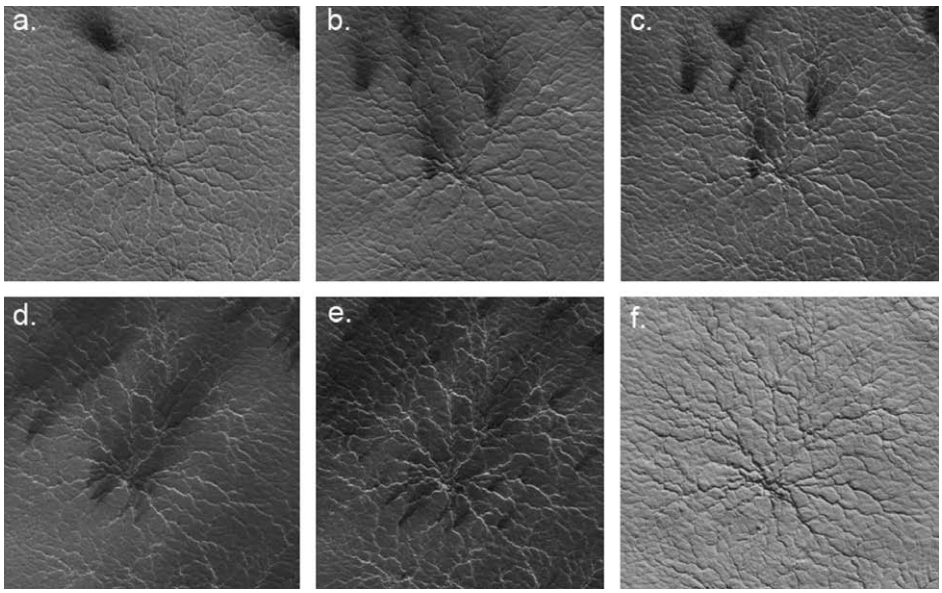

Fig. 16. The seasonal sequence of events is illustrated for the sublimation of a specific spider. Ls = 180 is the first day of spring in the southern hemisphere. (a) PSP_002532_0935, Ls = 181, shows that a few small fans have formed as the Sun starts to come above the horizon. (b) PSP_002850_0935, Ls = 195. Four dust fans (labelled 1, 2, 3, 4) have emerged from the spider's channels. Translucent ice is warmed from below, and evaporates below the seasonal ice layer. The gas finds a weak spot and vents to the top of the ice layer above, carrying dust from the surface along. The dust is blown around by the prevailing wind. (c) PSP_002942_0935, Ls = 200, shows the fans darkening. Dust gets trapped in the channels. The overall albedo darkens. (d) PSP_003496_0935, Ls = 226, shows that the wind direction has changed, the existing fans have lengthened, and there are numerous new fans coming from the channels as the overlying ice layer thins. (e) PSP_003641_0935, Ls = 233, has the lowest incidence angle in the set (70.7°). Most of the surface ice is gone. The channels are bright because the Sun is shining more directly on the walls. A thin lane of dark dust can be seen on the bottom of the largest channels. (f) PSP_005579_0935, Ls = 325, was taken well into southern summer, after all seasonal frost is gone. It is clear that channels are carved into the surface, not the seasonal ice. Fans have disappeared in the sense that they no longer contrast with the surface material that they came from in the first place. The surface material is water–ice cemented dirt covered with a layer around 5 cm deep of dessicated silt-sized dust, which is redistributed every season in this process of fan creation and deposition.

after year. Competing with this growth is the quantity of dust redistributed by the escaping gas, which may completely fill a channel. The spider shown in Fig. 16d has just a very narrow thin layer of darker dust in its channels (the bright sides of the channels are still visible and presumably not coated in a dark dust layer). In contrast, other channels elsewhere appear to be filled with dust that blankets the surroundings (e.g. Fig. 3). The texture of the surface adjacent to the channels suggests that channels form and grow, but may also fill and get choked off, then form new channels numerous times.

7.2. Fading of jet deposits

The HiRISE data set shows that jet and cryo-fumarole activity is initiated at almost all sites within the first 60 Sols of southern spring. After this time, activity appears to continue at some but not all of the previously established vents. Fan coverage of the surface increases. However, as the surface CO_2 frost deposit from the previous winter finally begins to disappear completely, the surface appearance undergoes a radical change (Fig. 17). In the images, the dark deposits appear to fade into the background. However, it is, of course, the bright surface which changes its reflectance with time. This can be illustrated graphically by taking the ratio of a bright area to that of a dark deposit (Fig. 18). This shows that at around Ls = 230° the surface under the seasonal ice becomes exposed. The exact timing will almost certainly depend upon the illumination and hence the local topography. The area studied to produce the plot in Fig. 18 is north-facing and hence one might expect removal of seasonal ice to be completed after this time in other areas.

To investigate this further, we have looked at CRISM observations. In Fig. 19, we have used two radiometrically calibrated CRISM spectral cubes (but not geometrically corrected) to assess changes in the surface CO_2 frost/ice distribution with time. The top panels show two spectral images (from cubes 4f9b and 74f9, left and right, respectively; see Table 1 for timing information and geometry) acquired at 1.245 μm. On the left, it can be seen that

Fig. 17. Image PSP_005426_0985 (Ls = 319°, LST = 15:25) showing a similar region to that seen in Fig. 1. By the time this image was acquired, much of the CO_2 frost accumulated in winter has sublimed. The dust particles produced by the jet and cryo-fumarole activity are now fading back into the background from where they will participate in another cycle of activity next year.

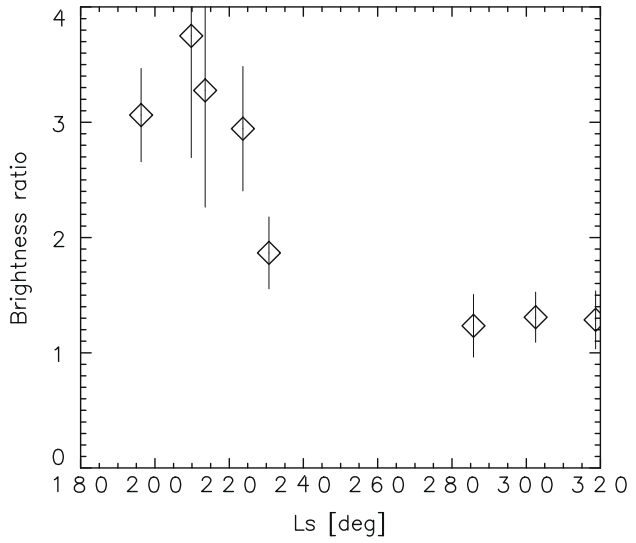

Fig. 18. The brightness ratio between a bright area and an adjacent dark deposit at a similar geometry using HiRISE observations. It can be seen that around Ls = 230° (orbit 3500), there is a sharp decrease in this ratio. The error bars indicate variations in the local brightness of the area used. This figure was compiled from a small area within the region covered by Fig. 2.

jet activity has left fan deposits over much of the surface. On the right, the fans have essentially gone, implying that surface ice has sublimed and that the dark deposits have returned to the substrate. We would expect therefore expect strong signatures of CO_2 surface ice for cube 4f9b and little or no surface ice in cube 74f9.

In the centre panels of Fig. 19, we show the 1.434 μm/1.245 μm ratios of the *I*/*F* values within the two cubes. A wavelength of 1.434 μm is within a major CO_2 absorption feature and at the wavelength used by Langevin et al. (2007) (within one pixel in wavelength) for the interpretation of OMEGA data. On the right, the image is bright and bland with few noticeable features. On the left, however, we only see bright regions where there are fan deposits and in the central depression region where there are a large number of active spiders. Elsewhere, the image is extremely dark. The image has been stretched linearly between a ratio of 0.6 and 1.1.

A wavelength of 1.434 μm is very close to the atmospheric CO_2 absorption band. However, this only reduces the illumination strongly – it cannot be responsible for a contrast reversal (unless there are extreme inhomogeneities in the atmospheric CO_2 distribution which are not physical). Hence, we are seeing additional absorption which is presumably from CO_2 ice on the surface which has not yet sublimed.

The lower panel shows the 1.703 μm/1.245 μm ratio. This illustrates that outside the CO_2 bands there is no contrast reversal. The image stretch here is between a ratio of 0.9 and 1.1 to enhance residual structure. This further suggests that the deposits appear to have faded into the background because the seasonal CO_2 ice layer has sublimed.

A remaining possibility is that the CO_2 ice remains but becomes covered with a layer of dust which is optically thick at visible and infra-red wavelengths. This can, with a fairly high degree of

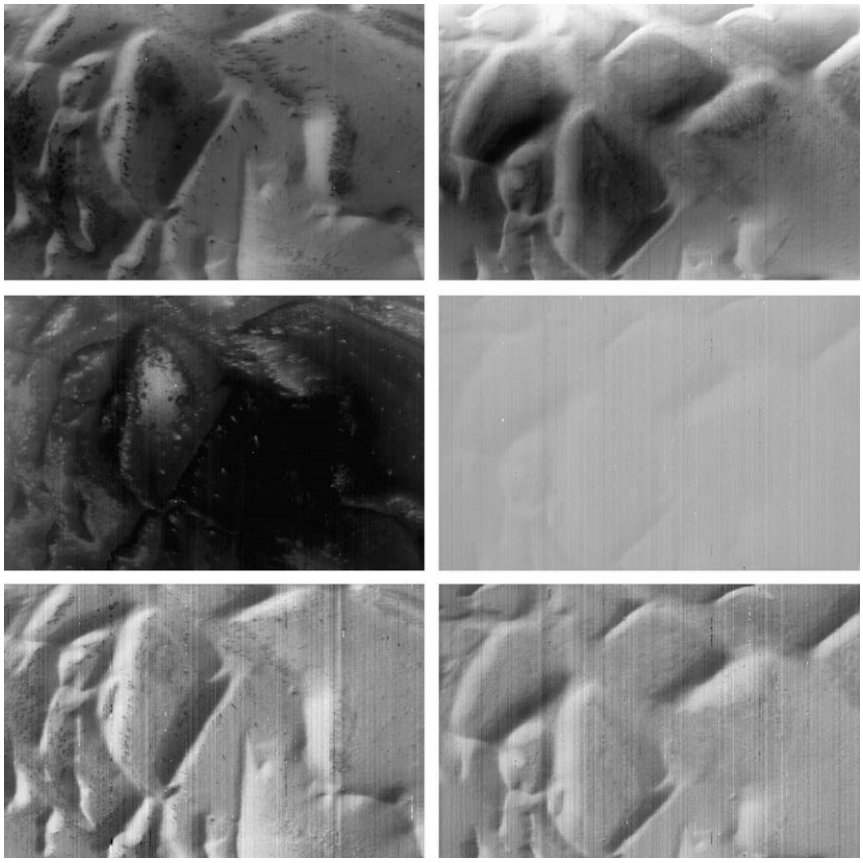

Fig. 19. CRISM observations of Inca City. Top: Spectral image at 1.245 μm. Centre: I/F ratio 1.434 μm/1.245 μm linearly scaled between 0.6 and 1.1. Bottom: I/F ratio 1.703 μm/1.245 μm linearly scaled between 0.9 and 1.1. Images to the left are products of CRISM image 4f9b. Right: 74f9. Note that most dark features in the top panel are bright in the centre left panel but not in the centre right panel. The region shown is around 9 km × 4 km (although the data are strongly geometrically distorted in this representation).

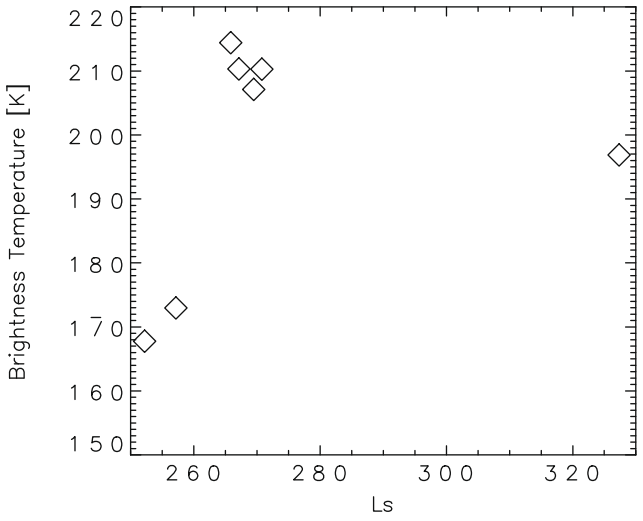

Fig. 20. THEMIS brightness temperatures for the Inca City region. The steep rise in temperature around Ls = 260° suggests that the CO_2 ice had completely sublimed at this time. The data were also acquired during the 2007 southern spring but at a much lower resolution than the HiRISE data.

certainty, be ruled out by looking at the THEMIS brightness temperatures for the region (Fig. 20) which should be compared with Fig. 18. The THEMIS temperatures rise somewhat later than the HiRISE brightness ratios but we repeat that the brightness ratios produced in Fig. 18 came from a north-facing slope which may therefore have lost its CO_2 earlier when compared to most of the rest of the region.

8. Conclusions and discussion

The Kieffer model of sublimation-driven jet activity producing dark dust deposits on top of a gradually thinning seasonal CO_2 ice slab is, in general, supported by HiRISE monitoring of specific regions near the southern polar cap. There are, however, details which suggest additional modeling studies are required.

In the Inca City region, there is clear evidence for the importance of topography in controlling sublimation-driven erosional processes. Firstly, araneiform (spider-like) structures on the surface are confined to areas of low local slope. Secondly, slopes have a cracked appearance and many of these cracks appear to be sources for dust emission throughout the early weeks of southern spring. There is no obvious explanation forthcoming from the images as to why some of these features should produce jet-like activity and others not. Thirdly, boulders on the tops of the ridges in the region are frequently surrounded by darker deposits and, early in the southern spring, by brighter bluer deposits which suggest weak dust emission and transport. In all these cases, the putative source of jet activity can often be recognised (even if the source cannot be precisely localised in some examples) towards the end of southern summer, even after the contrast between the emitted dust and the background has been lost. There are, however, regions of low slope where dust deposits originate in quasi-linear sources. Here there are no obvious signatures of the nature of these sources remaining once the CO_2 ice has fully sublimed. The topographic context clearly plays a substantial role in determining the type of activity that occurs. Activity at spiders initiates at depression boundaries possibly as a result of stress on the CO_2 slab ice at these points. Erosion by gas flow at these points increases the size of the spider. On slopes, cracks dominate the observed activity and a gravitational influence might be inferred. On flat, topographically smooth regions, linear cracks are evident, which may be the result of pressure build-up and cracking of a fairly uniform CO_2 ice slab.

Some sources of outgassing appear to be able to re-charge. The process by which this can be achieved is not known although candidates include (1) the vent may reseal itself by some process which is not known (although annealing of small diameter vents/holes might be feasible; Kieffer, 2007), (2) outgassing may occur episodically when individual sub-surface channels become open, (3) the insolation and gas production may be strong enough to produce eruptions over a full diurnal cycle so that outgassing and dust deposition is a continuous process modulated by the insolation until all CO_2 ice has been used up (Kieffer et al., 2000; Titus et al., 2008), (4) there could be superposition of two or more vents in close proximity such that it becomes impossible to distinguish the individual sources even at HiRISE resolutions, (5) as the slab ice thins the albedo may decrease leading to enhanced energy absorption which further fuels sublimation from the base, (6) the CO_2 ice slab may open and close itself by a lifting process depending upon the pressure under the slab. A combination of these mechanisms cannot be ruled.

Ventings in some areas are more akin to ground-hugging flows, the directions of which are topographically controlled. This leads to patchy deposits which are also influenced by the local topography.

There is strong evidence that HiRISE has captured images of several jets in progress. In the event that this interpretation is correct, a minimum dust production rate of 30 g s^{-1} has been derived for an individual source although the uncertainties suggest that values up to three orders of magnitude higher might be possible. The observed activity occurred late in the afternoon which further indicates that activity is initiated and maintained by a complex combination of influences.

Acknowledgments

The comments of two anonymous referees led to a significant improvement in the manuscript as did further comments from the Editor. Thanks to Alexandra Lefort for reduction of the THEMIS data seen in Fig. 20. Also thanks to the HiRISE science ops team for their efforts to implement the observing plan. This work has been supported in part by the Swiss National Science Foundation.

References

Aharonson, O., Zuber, M.T., Smith, D.E., Neumann, G.A., Feldman, W.C., Prettyman, T.H., 2004. Depth, distribution, and density of CO_2 deposition on Mars. J. Geophys. Res. 109, E05004. doi:10.1029/2003JE002223.

Bohren, C.F., Huffman, D.R., 1998. Absorption and Scattering of Light by Small Particles. John Wiley & Sons, New York.

Delamere, W.A., and 15 colleagues, this issue. Color Imaging of Mars by the High Resolution Imaging Science Experiment (HiRISE). Icarus 205, 38–52.

Graf, J.E., Zurek, R.W., Eisen, H.J., Jai, B., Johnston, M.D., Depaula, R., 2005. The Mars reconnaissance orbiter mission. Acta Astronautica 57, 566–578.

Hansen, C.J., Thomas, N., Portyankina, G., McEwen, A., Becker, T., Byrne, S., Herkenhoff, K., Kieffer, H., Mellon, M., this issue. HiRISE Observations of gas sublimation-driven activity in Mars' southern polar regions: I. Erosional Features on the Surface. Icarus 205, 283–295.

Henning, T., Il'in, V.B., Krivova, N.A., Michel, B., Voshchinnikov, N.V., 1999. WWW database of optical constants for astronomy. Astron. Astrophys. 136 (Suppl.), 405.

Johnson, T.V., Matson, D.L., Blaney, D.L., Veeder, G.J., Davies, A., 1995. Stealth plumes on Io. Geophys. Res. Lett. 22, 3293–3296.

Kaufmann, E., 2007. PhD Thesis, Technical University of Graz.

Kaufmann, E., Komle, N.I., Kargl, G., 2006. Laboratory simulation experiments on the solid-state greenhouse effect in planetary ices. Icarus 185, 274–286.

Kieffer, H.H., 2000. Annual punctuated CO_2 slab-ice and jets on Mars. Paper Presented at the 2nd International Conference on Mars Polar Science and Exploration, 21–25 August. University of Iceland, Reykjavik. p. 93.

Kieffer, H.H., 2007. Cold jets in the martian polar caps. J. Geophys. Res. (Planets) 112, 8005. CiteID Eo, doi:10.1029/2006JE002816.

Kieffer, H.H., Titus, T.N., Mullins, K.F., Christensen, P.R., 2000. Mars south polar spring and summer behavior observed by TES: Seasonal cap evolution controlled by frost grain size. J. Geophys. Res. 105, 9653–9699.

Kieffer, H.H., Christensen, P.R., Titus, T.N., 2006. CO_2 jets formed by sublimation beneath translucent slab ice in Mars' seasonal south polar ice cap. Nature 442, 793–796. doi:10.1038/nature04945.

Kirk, R.L., Soderblom, L.A., Brown, R.H., Kieffer, S.W., Kargel, J.S., 1995. Triton's plumes: Discovery, characteristics, and models. In: Cruikshank, D.P. (Ed.), Neptune and Triton. University of Arizona Press, pp. 979–989.

Langevin, Y., Bibring, J.-P., Montmessin, F., Forget, F., Vincendon, M., Doute, S., Poulet, F., Gondet, B., 2007. Observations of the south seasonal cap of Mars during recession in 2004–2006 by the OMEGA visible/near-infrared imaging spectrometer on board Mars Express. J. Geophys. Res. (Planets) 112, 8. doi:10.1029/2006JE002841.

Leighton, R.B., Murray, B.C., 1966. Behavior of carbon dioxide and other volatiles on Mars. Science 153, 136–144.

Malin, M.C.and 15 colleagues, 1998. Early views of the martian surface from the Mars Orbiter Camera of Mars Global Surveyor. Science 279, 1681–1685.

Malin, M.C., and 13 colleagues, 2007. Context Camera Investigation on board the Mars Reconnaissance Orbiter, J. Geophys. Res. (Planets), 112, CiteID: E05S04, doi:10.1029/2006JE002808.

Matson, D.L., Brown, R.H., 1989. Solid-state greenhouses and their implications for icy satellites. Icarus 77, 67–81.

McEwen, A.S., and 14 colleagues, 2007. Mars Reconnaissance Orbiter's High Resolution Imaging Science Experiment (HiRISE). J. Geophys. Res. (Planets), 112, CiteID: E05S02, doi:10.1029/2005JE002605.

McEwen, A.S., and 68 colleagues, this issue. The High Resolution Imaging Science Experiment (HiRISE) during MRO's Primary Science Phase (PSP). Icarus 205, 2–37.

Murchie, S., and 49 colleagues, 2007. Compact Reconnaissance Imaging Spectrometer for Mars (CRISM) on Mars Reconnaissance Orbiter (MRO). J. Geophys. Res. (Planets) 112, CiteID: E05S03, doi:10.1029/2006JE002682.

Paige, D.A., Keegan, K.D., 1994. Thermal and albedo mapping of the polar regions of Mars using Viking thermal mapper observations, 2. South polar region. J. Geophys Res. 99, 25993–26013.

Piqueux, S., Byrne, S., Richardson, M.I., 2003. Sublimation of Mars's southern seasonal CO_2 ice cap and the formation of spiders. J. Geophys. Res. 108 (8), 5084. doi:10.1029/2002JE002007.

Piqueux, S., Christensen, P.R., 2008. North and south subice gas flow and venting of the seasonal caps of Mars: A major geomorphological agent. J. Geophys. Res. (Planets) 113, CiteID E06005, doi:10.1029/2007JE003009.

Portyankina, G., 2006. PhD Thesis, Atmosphere-surface vapor exchange and ices in the Martian polar regions, Georg-August-Universität, Göttingen.

Portyankina, G., Hansen, C.J., Markiewicz, W.J., Thomas., N., this issue. HiRISE observations of gas sublimation-driven activity in Mars' southern polar regions: III. Models of processes involving translucent ice. Icarus.

Strom, R.G., Schneider, N.M., 1982. Volcanic eruption plumes on Io. Satellites of Jupiter. University of Arizona Press, Tucson. pp. 598–633.

Titus, T., Kieffer, H.H., Langevin, Y., Murchie, S., Seelos, F., Vincendon, M., 2007. Bright fans in Mars' cryptic region caused by adiabatic cooling of CO_2 gas jets. AGU (abstract P41A-0188).

Titus, T.N., Calvin, W.M., Kieffer, H.H., Langevin, Y., Prettyman, T.H., 2008. Martian polar processes, In: Bell, J.F., III (Ed.), The Martian Surface: Composition, Mineralogy, and Physical Properties. Cambridge University Press, ISBN 9780521866989 (Chapter 25).